Reliability Testing of Shingle-Matrix Modules in Glass-Glass Construction

Marc-Philipp Bauer[1,*]

[1]Dresden, Germany

*Correspondence: Marc-Philipp Bauer, marc-philipp.bauer@outlook.com

Abstract. Solar modules utilizing Shingle-Matrix-Technology present a promising opportunity for the future of European solar module manufacturers due to their technological benefits compared to the Asian mainstream [1]. To fully exploit their potential, Shingle-Matrix modules must demonstrate exceptional reliability. To assess their reliability, glass-glass Shingle-Matrix modules were manufactured, tested, and subjected to two years of outdoor exposure and standardized testing conditions in accordance with IEC 61215 [2]. The results were subsequently compared to modules with conventional architecture. The tested shingle-matrix-modules demonstrated resilience to the certification tests. By repeating and combining standard test routines beyond IEC the modules resilience was studied further. The Shingle-Matrix modules consistently yielded results that remained well within the established performance parameters. This outcome demonstrates the potential for a IEC certification-compliant market introduction, as demonstrated through the selected validation tests. The module's aesthetic design and shading resilience contribute to its suitability for building integrated photovoltaics (BIPV).

Keywords: Solar Module, Shingle Matrix, Reliability Testing, Photovoltaics, BIPV

1. Introduction

Shingle-Matrix-Technology is an interconnection technology for solar cells. Stripes of solar cells are joined together by applying electrically conductive adhesive and arranging them in an overlapping fashion comparable to roofing shingles. After curing a shingle-matrix is formed. It excels in comparison to other methods by not using lead containing ribbons, being more shading resilient than butterfly-modules and achieving the highest aesthetical appeal [1]. Within Shingle-Matrix-Modules the matrix is created by interconnecting the stripes of solar cells in such a way that each cell stripe of a row of cell is connected in parallel, and each row of cell stripes is connected in series with the next row. For shingle string modules the stripes are connected in series as strings and afterwards joined in parallel.

In recent years, solar cells have changed widely in size, busbar-count, and technology [3], [4]. These changes will force module manufacturers to repeatedly change their interconnection machines, i.e. stringers to stay competitive and utilize the improved cell efficiency as described by Schachinger [5].

As a Shingle-Matrix-Stringer does not rely on busbars and is flexible in regard of the cell dimension it could loosen the dependency on cell manufacturers by keeping their solar-cells specs identically. This can be seen as an opportunity for European solar manufacturing entities to reshore the manufacturing of solar modules. And futureproof it for emerging cell technologies [6]. To ensure suitability for field deployment, the modules must undergo rigorous

reliability testing, ensuring that end customers receive a high-quality product capable of meeting their energy needs over an extended lifespan.

The purpose of this paper is to shed light on the reliability of shingle matrix technology solar modules with glass-glass construction. First, the materials and methods used in this paper are presented. This is followed by the results of reliability tests. These results are then discussed and put into perspective from a manufacturing and product point of view.

2. Materials and Methods

2.1 Reliability testing

Solar module manufacturers periodically conduct reliability tests on all prototypes and on high volume products to ensure only high-quality products will reach the customer. These tests are performed according to i.e. IEC 61730 [7] and IEC 61215 [2]. Often, the specified cycle count is exceeded to provoke degradation results and to detect flaws in the module design or material choice and the resulting module bill of materials (BOM).

As reliability tests the following tests were performed and evaluated for this paper to test the module reliability:

- Performance at STC (MQT 06.1 [7])
- Stabilization via LID (MQT 19 [2])
- Thermal-cycling test TC200 (MQT 11 [2])
- Damp-heat test DH1000 (MQT 13 [2])
- Static mechanical load test SML (MQT 16 [2])

For the SML test the modules were mounted horizontally, in portrait mode, clamped onto two rails located 240 mm from the short side of the module as seen in Figure 1. The module was loaded consecutively with +8.6 kPa and -3.6 kPa.
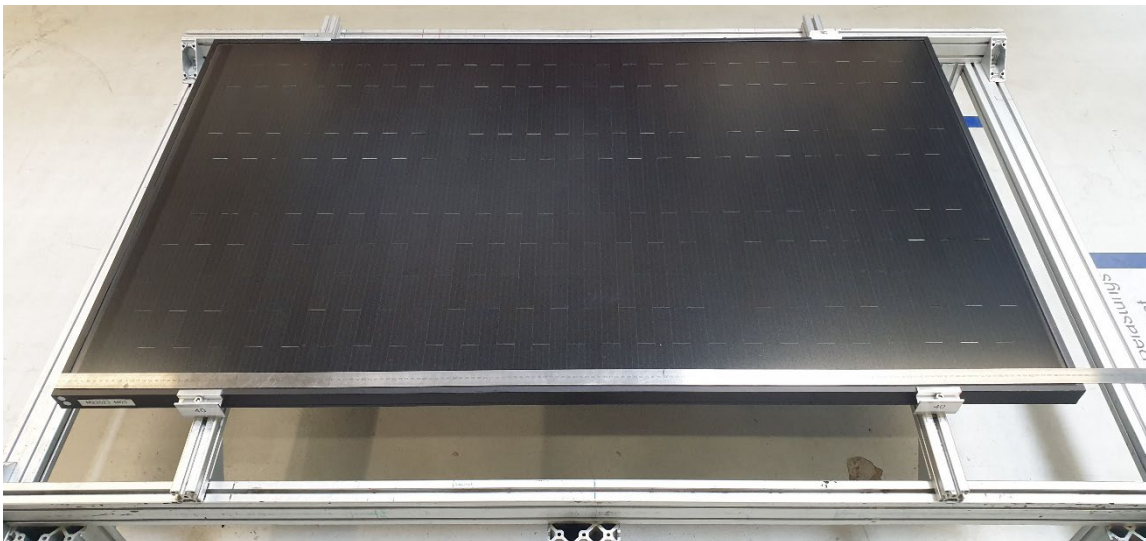

Figure 1. Solar module mounted for SML test

Repetitions of the standardized climate chamber tests like TC and DH were performed within this research. The datasets are marked with the total test exposure at that evaluation time. i.e., a module with TC400 was subjected to two TC200 tests and endured 400 cycles whereas a module that endured DH2000 was subjected to 2000 h of Damp heat exposure.

Whereas repetitions of the SML test were not incremented in the experiment naming as those loads are not summative.

Two shingle-matrix modules were mounted on an outdoor exposure rack in Dresden (Germany) facing SSE at a 40° inclination and connected to an MPPT micro-inverter as ballasts. The photograph, figure 2, highlights the mounting clamp position and aluminum extrusions, placed near one module side to maximize wind and snow-induced deformation and potential defects. The modules were removed once per year and brought into the laboratory for performance evaluation and were afterwards remounted.
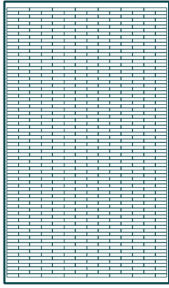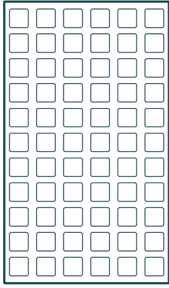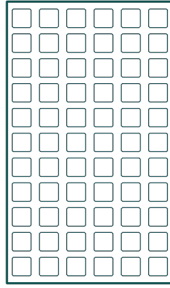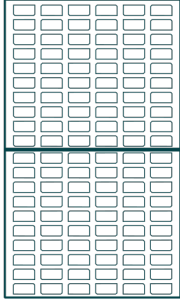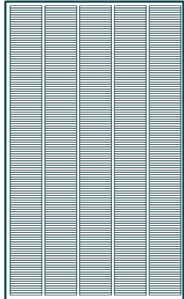

Figure 2. *M1 and M2 (modules in the center) during Outdoor exposure with identically sized modules, mounted regularly on each other side*

The test progressions were especially selected to verify known failure prone tests observed by Klasen et. al. [8], Rößler et. al. [9], Foti et. al. [10], and Zahn et. al. [11] i.e. SML, TCT, and DHT.

2.2 Modules

Shingle-Matrix-Modules (SM) were manufactured and tested. The results were compared to results from commercial modules. Table 1 compares the different modules regarding their main parameters. The modules were chosen to have the most common parts of the BOM. i.e. the Shingle-Matrix, F7-SiON and F7 [12] are based on the same aperture-size and share many materials with each other. The F8 [13] module was chosen, as it is the successor to the F7 product line and shares many components. The Modules were manufactured by Solarwatt GmbH. Finally, a commercial Shingle-String module was chosen as a benchmark product.

Table 1. Comparison between the tested modules and their main parameters. (left to right) Shingle-Matrix (SM), Vision 60 M Construct (F7-SiON), Vision 60M Construct (F7), Vision GM 3.0 (F8), Shingle-String (SP)

	Shingle-Matrix	F7 SiON	F7	F8	Shingle-String
Size w., l. [mm]	1000 1700	1000 1700	1000 1700	1052 1780	1085 1808
Mpp [Wp]	310	310	310	365	405
Cell	PERC (Mono) shingle matrix	PERC (Mono) SiON 5BB	PERC (Mono) 5BB	PERC (Bifi) 9BB	PERC (Mono) shingle string
Cell format	G1 1/5	M2	M2	M6 ½	G12 1/6
Connect.	ECA-overlap	Flat ribbon	Flat ribbon	Round wire	ECA-overlap
EBM	EVA-A	EVA-A	EVA-B	EVA-A	n.a.
Constr.	G/G, ARC 2mm/2mm	G/G ARC 2mm/2mm	G/G ARC 2mm/2mm	G/G ARC 2mm/2mm	G/F 3.2mm/-
Frame [mm]	40	40	40	40	30
Datapoint	2022-2024	2021	2021	2022	2024
SML load [kPa]	+8,1 -3,6	+8,1 -3,6	+8,1 -3,6	+8,1 -3,6	+5.4 -2,5

3. Results

3.1 General results

Figure 3 illustrates the order and tests performed for each module family. Figure 4 shows the corresponding electrical measurements results. The order is identical between the two figures. It is noteworthy that all modules are within the >-5% limit defined by IEC and degrade only a minor amount at sampling-time after TC200. The Shingle-Matrix module shows a degradation of -0.03% (P_{MPP}). The F7-SiON module degraded by -2.3% (P_{MPP}). The degradation in fill-factor (FF) happens in similar matter. The F7 and F8 Module start to show signs of degradation after TC400. The Shingle-Matrix module still stays within -0.24% of the initial Peak-Power (P_{MPP}). The Shingle-String module surpasses the IEC limit of -5% (P_{MPP}) and exhibits a power loss of -8.1% (P_{MPP}), -5.6% (FF) and a voltage drop of -3% (UOC).
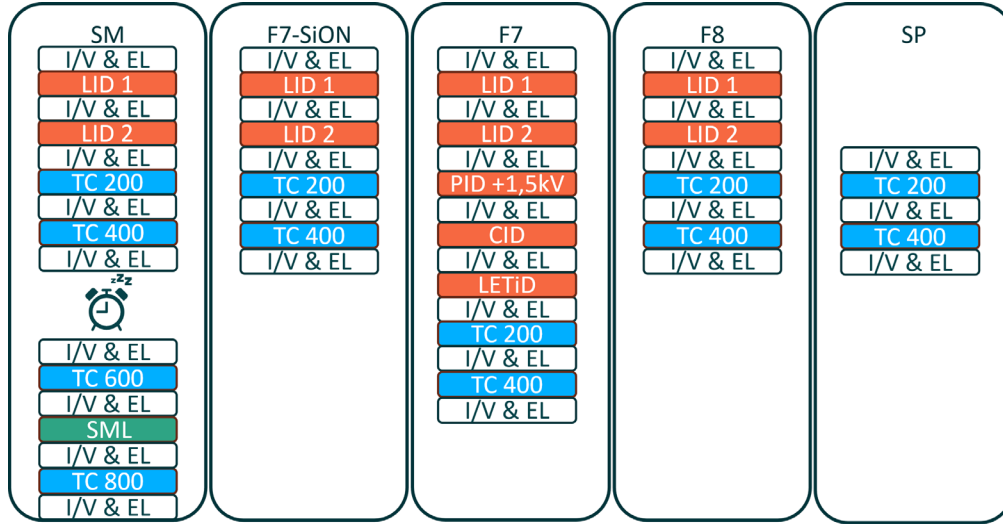
Figure 3. *Flow Chart of five module-types (l. to r.: SM, F7-SiON, F7, F8, SP) with their tests: LID (used for stabilisation), PID, CID, LETiD, SML and EL & I/V testing*
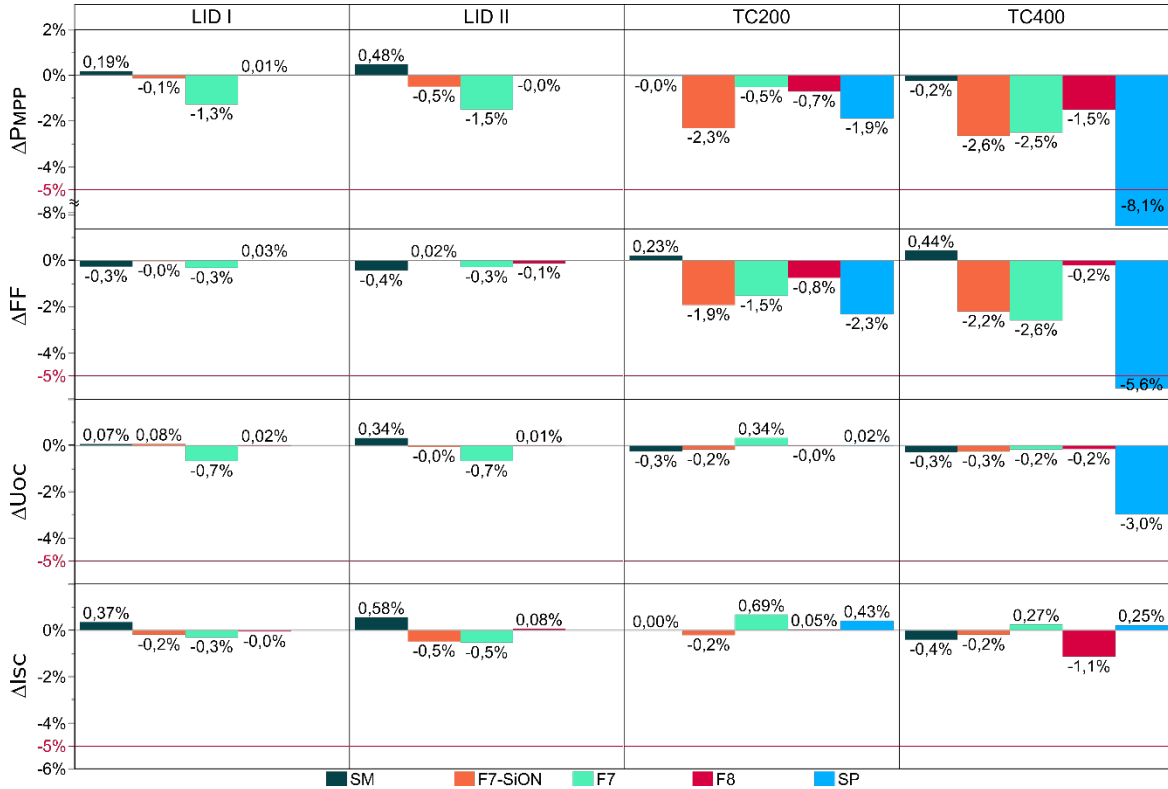

Figure 4. *Normalized test results TC-testing (init. = 0), dataset order like Figure 3 in each sub-plot (l. to r.: SM, F7-SiON, F7, F8, SP)*

In Figure 5 one can find the flow chart for a second set of modules and their endured reliability tests. Figure 6 shows the corresponding electrical characteristics after each test. The order of the modules is corresponding to each sub-plot. From this samples data the DH-testing was affecting the modules performance the most. After 1000h the degradation was almost -2% at P_{MPP}. In this subplot the SM module degraded by -2.7% (P_{MPP}). The F7 module on the other hand degraded by -1.8% (P_{MPP}) which decreased to -5.7%(P_{MPP}) after dark storage conditions. The IEC norm permits for this cell type a light induced healing cycle which regenerated the module to +1.26% (P_{MPP}). An I_{SC} reduction of less than -1.7% can be seen for all modules after the DH1000 test. The following SML test has only a minor impact on the module performance. Within the DH2000 test the modules degrade further but only with

decreased gradient. Nevertheless, all modules stay well within the -5% margin defined by IEC. One shall be aware that the Shingle-Matrix-Module has endured the DH2000-Test before being subjected to the SML-test as displayed in Figure 5.
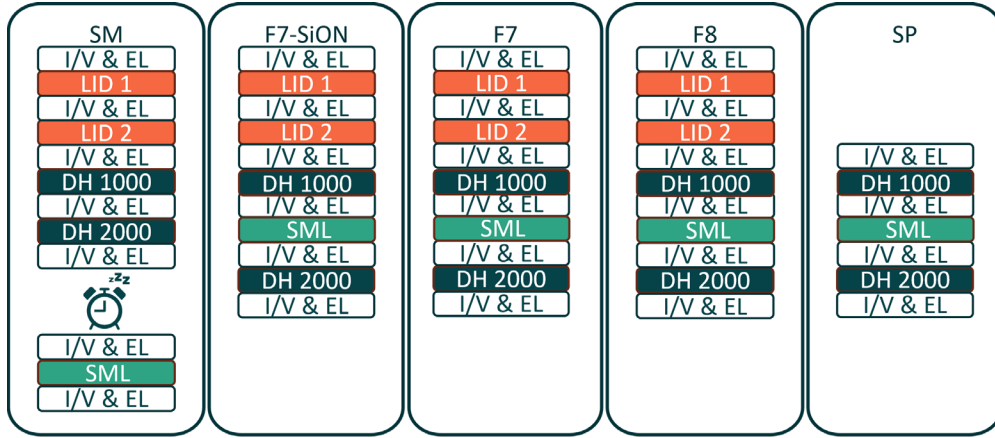

Figure 5. *Flow Chart of five module-types (l. to r.: SM, F7-SiON, F7, F8, SP) with their tests: LID (used for stabilization), DH1000, SML and EL & I/V testing.*
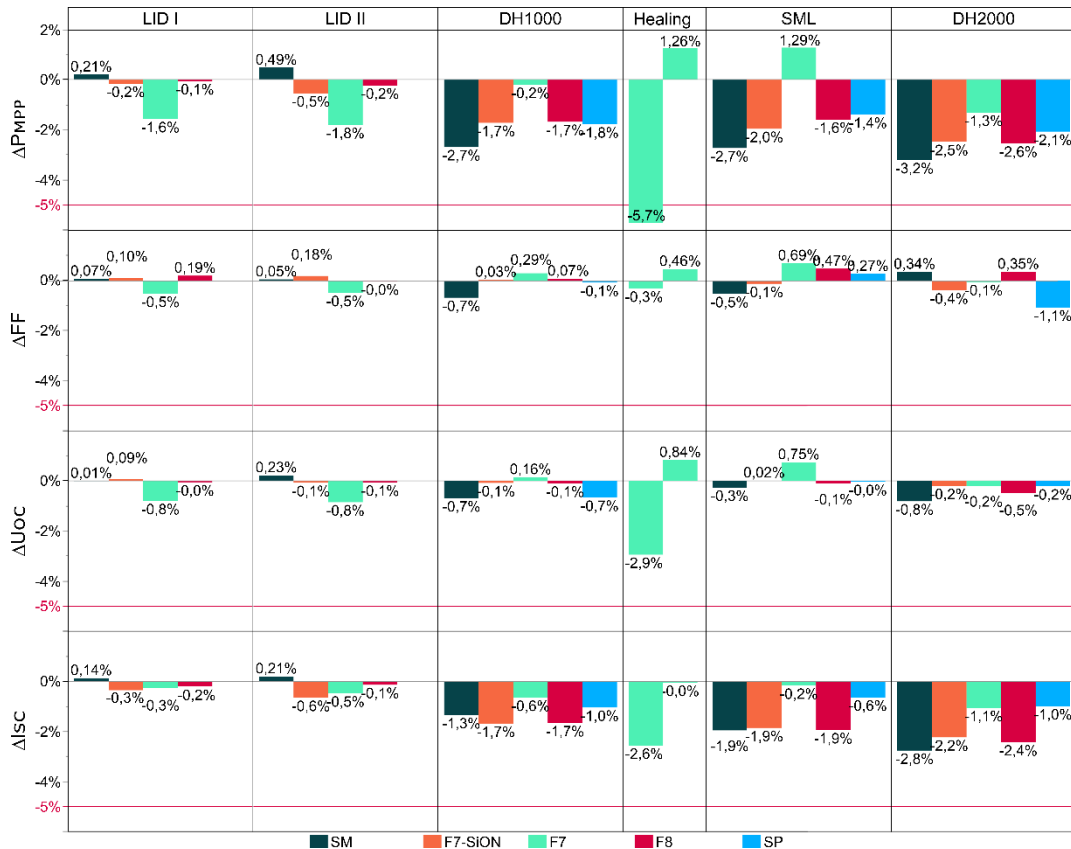

Figure 6. *Normalized test results DH and SML (init. = 0), dataset order like Figure 5 in each sub-plot (l. to r.: SM, F7-SiON, F7, F8, SP)*

3.2 Detailed results for Shingle-Matrix-modules (GEG)

For a more detailed comparison between the shingle-matrix modules, their testing regime is aggregated in Figure 7. Their resulting performance data can be viewed in Figure 8. General comparison to the other module types were given in the previous chapters. This section displays additional findings.
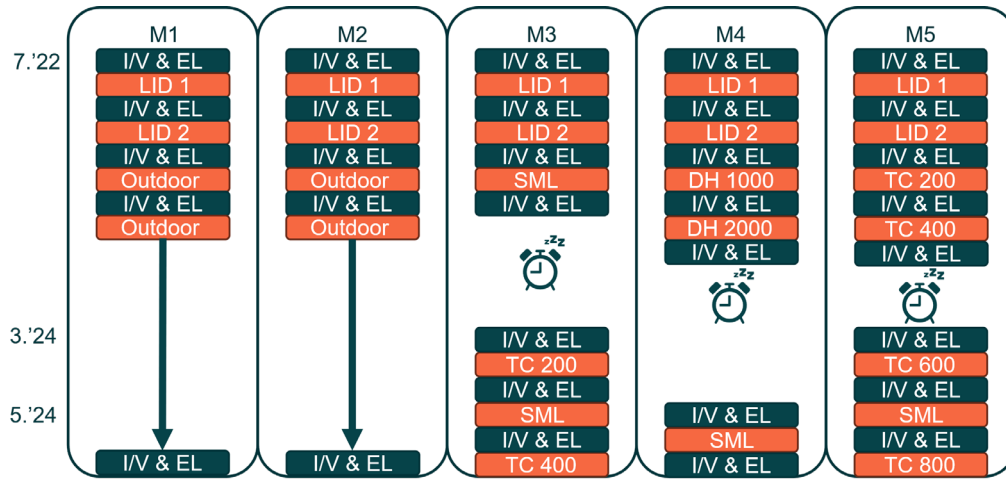
Figure 7. *Reliability tests of five Shingle-matrix-modules (M1...M5), whereas M1 and M2 were subjected to outdoor testing, M3 and M5 were subjected to SML and TC test and M4 was subjected to DH test and SML.*
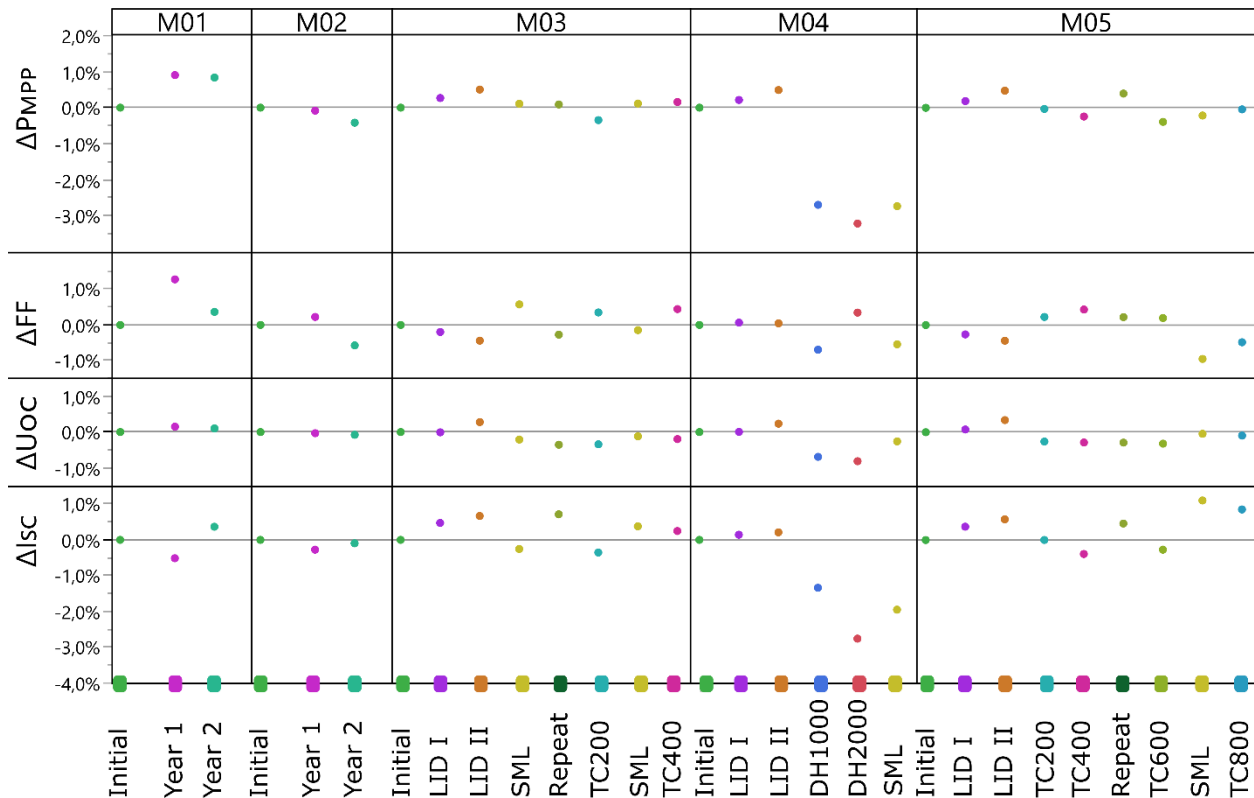

Figure 8. *Normalized test results (initial = 0) for all Shingle-Matrix-Modules. Datapoints are ordered similarly to Figure 7*

3.2.1 Outdoor testing

EL images taken before, during, and after exposure showed no significant brightness changes, no new (micro) cracks, or progression of existing damage, particularly in the connecting areas occurred. Electrical measurements, as shown in Figure 8, confirmed the expected module performance. With little to no degradation.

3.2.2 SML and Thermal Cycling Tests

Module 3 and Module 5 were subjected to SML and TC tests. The electrical characterization revealed a slight degradation of the module parameters during SML after TC600, particularly a -0.95% decrease in FF. The EL pictures exhibited minor indications of cell degradation, and on Module 5, a persistent seed crack propagated during the final SML test, as illustrated in Figure 9. One can observe the changes in EL-emissivity after the TC800 testing in the center of Figure 9. Noteworthy here the shift in Brightness between the defective shingle and its neighbors where the current is redistributed to.
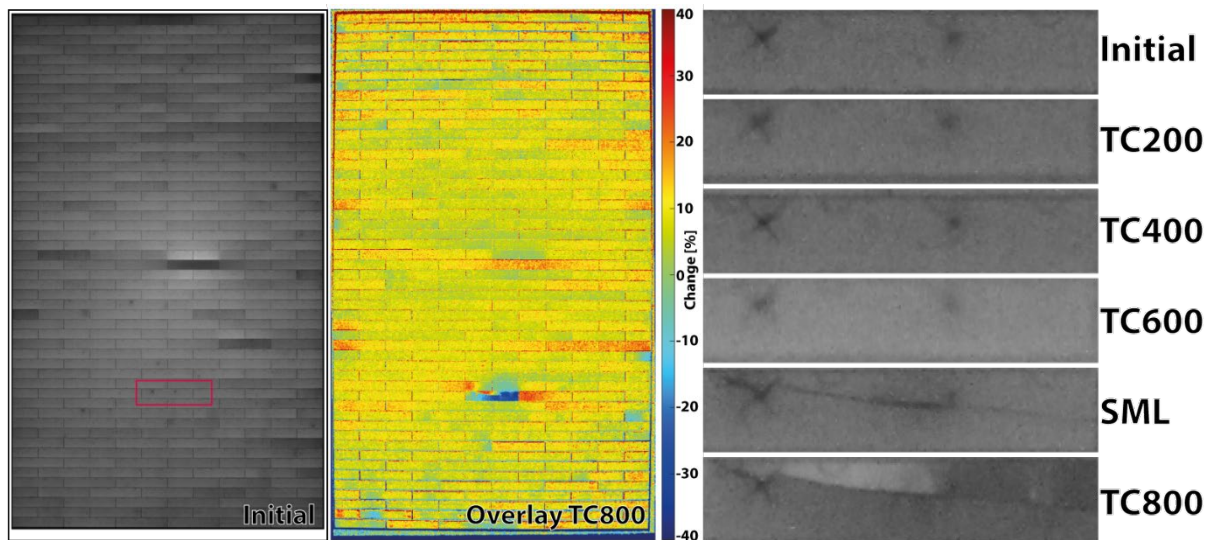

Figure 9. *EL-pictures of Shingle-Matrix-Module M05 during testing sequence (left: inital, center: EL overlay of initial and post TC800, right: progression of seed-crack)*

3.2.3 SML and Damp Heat Tests

Module 4 was subjected to DH testing and SML after the initial stabilization. This module showed signs of glass corrosion after the first 1k hours of the DH test sequence, which occur in certain cases during the DH tests. The glass corrosion affects primarily the ARC on the front surface and alters the surface quality of the module glass. Its visual appearance can be compared to water stains (see Figure 10 right) but are permanent and affect the light-in-coupling by reducing the transmissivity of the glass surface. This phenomenon can be observed during power measurements by the reduced short-circuit current (-2.8% I_{SC}), which is usually connected to the irradiance. In the center of Figure 10 the overlay displays the EL-Emissivity changes over time. Unfortunately, the overlayed image is not ideal as one can see from the image artifacts in the bottom and top of the graphic. The EL picture shows limited brightness changes one some cells and a crack, which was present since manufacturing and extended into a V-crack during the SML test.
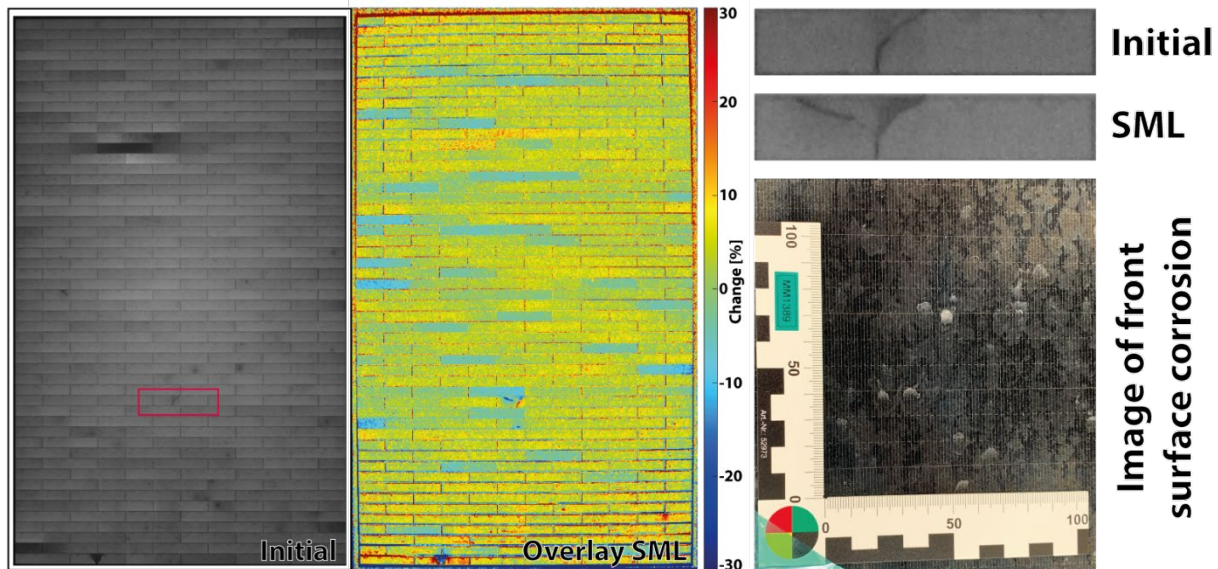
Figure 10. *EL-pictures of Shingle-Matrix-Module M04 during testing sequence (left: initial, center: EL Overlay of initial an post SML, right:progression of seed-crack), right bottom: picture of surface corrosion after DH2000 on front glass*

4. Discussion

As to the author's knowledge, the tested Shingle-Matrix-Modules were the first full format modules with glass-glass construction. The Shingle-Matrix-Modules display a high resilience towards power degradation within combined tests of SML and TC-Tests compared to conventional flat-ribbon and round-wire ribbon modules and display comparable degradation during DH-testing as shown in Figure 4 and Figure 6.

The present study was conducted within the constraints imposed by a manufacturing company, a circumstance that has imposed certain limitations on the scope and rigor of the research. These limitations are primarily associated with the availability of resources for prototyping and testing, as well as the precise determination of the absolute module performance. All characterizations were performed internally in the same VDE (Verband der Elektrotechnik Elektronik Informationstechnik e. V.) accredited laboratory. All performance data were obtained by comparative measurements with traceable golden standard modules but due to the differences in the test subjects' construction and materials, only relative changes of the modules are discussed here. Another limitation is the sample size as it might affect statistical power and robustness of the conclusion. Thus, the datapoints can only be seen as performance indicators. Thirdly, as evidenced by the EL-Pictures displayed, these modules exhibit a high degree of nonuniformity. Given that the shingle matrix modules were produced during the initial acceptance of the stringing demonstrator tool, numerous process optimizations had yet to be implemented. A comparison of the EL-Pictures in this study to those in recent publications, such as Latif et al. [14], reveals a substantial improvement in the initial condition. The initial defects should have a negative impact on performance, as they impede the modules' capacity to redistribute current flows.

The TC tests as shown in Figure 4 create changing levels of internal stress within the structure of the module by thermally expanding and contracting all materials. This can be observed especially on the interface between the ribbons and cells as described by Charpentier et. al. in [15]. The observed effects can be attributed to the dissimilar coefficients of thermal expansion between silicon and copper. A rule of thumb can be derived from the data, suggesting that a reduction in concentrated copper matter is desirable. This can be achieved through either an overall reduction or a more effective distribution of copper matter. However, both methodologies are associated with their own set of challenges. For instance,

the ribbon-cross-section reduction leads to increased resistivity, while a more decentralized distribution of copper results in increased shading and necessitates greater production efforts. This can be seen in the evolution of the available modules where a 5BB module (F7) performs worse than a 9BB module (F8) during TC tests. In contrast, shingling can be a viable option due to its significantly reduced need for interconnections, with those connections positioned between two flat surfaces of similar material. Despite the overlap of cells, there is an absence of shading of inactive components.

In contrast, the shingle-string module shows larger defects, especially on the solar cells with attached cross-connectors. - This is an area where copper busbars are i.e., soldered to silicon cells. Since they are located at the perimeter of the module, edge effects, i.e. thinning of the encapsulant, reduced ability to distribute mechanical stress, and higher initial stress, are believed to play a critical role in creating nuclei for cell crack propagation. After TC200, cell defects in the shingle string module increase rapidly and are uniformly distributed. One would associate these defects with a semi-optimal shingle joint in conjunction with the glass-foil construction of the module, as described by Klasen [8], for example.

On the other side in one Shingle-Matrix-Module (M5) a crack propagated after TC600 and SML. This crack is worth noting, as it did not propagate along the typical 45° trajectory. It followed the strain iso lines described by for example Beinert et. al. [16]. Other persistent seed cracks did not propagate during this testing period. This shows how well the glass-glass construction protects the cells against bending loads and distributes stress. Although single cells were rendered ineffective the impact on the module performance was negligible. Due to the module's intrinsic parallel interconnection scheme, disruptions in the current path can be effectively redistributed across the intact shingle interconnections.

After DH testing, all modules exhibit a reduction in short-circuit current (ISC) as seen in Figure 6. This can be attributed to a combination of cell degradation induced by persistent acetic acid from the ethylene-vinyl acetate as described by Irikawa et. al. [17] and in this case glass corrosion of the front glass, the latter manifesting with water stain-like defects forming on the anti-reflective coating (ARC) and thus reducing the cell irradiance as seen in Figure 10. The EL-Pictures of the corresponding Shingle-Matrix-Module show comparable intensities and marginal signs of non-uniform cell degradation. As acetic acid induced cell degradation normally affects the non-passivated shingle wafers perimeters first. Nevertheless, even after doubling the required DH testing interval, all module types remain well within the acceptable degradation range.

Shingle-matrix modules can play a crucial role as they deliver highly aesthetic and performant solar active surfaces and performed tests indicate excellent performance reliability. For building-integrated photovoltaic (BIPV) systems, both an aesthetically pleasing appearance and long service life are essential. Facade defects and maintenance are associated with significant effort, cost, disruption and risk to the building. Several approaches have already been developed to enhance the durability of these modules. These include low-damage separation techniques followed by edge passivation, as described by i.e., Lohmüller [15]. The use of inert encapsulation films, and improved sealing against water vapor migration should be investigated next. Such measures can further enhance the reliability of Shingle-Matrix modules.

All these approaches have already been implemented in different series products and can be combined and scaled to an industrial level for use in BIPV modules. Additionally, the integration of newer cell technologies such as TopCon, HJT, or tandem cells offer further potential to improve the energy yield of Shingle-Matrix modules by increasing conversion efficiency and enhancing low-light performance. With these advancements, Shingle-Matrix modules can be highly suitable for long-term use in building-integrated photovoltaic systems.

5. Conclusion

Within this research it is shown that Shingle-Matrix-Modules can endure damp heat (DH), thermal cycling (TC), mechanical load (SML) testing and combined sequences of these tests and still perform well within the limits defined by IEC 61215.

The findings highlight the advantages of the Shingle-Matrix design, particularly its ability to mitigate localized defects through intrinsic parallel interconnections, ensuring stable electrical performance even under challenging conditions.

Despite initial process-related irregularities, the glass-glass construction of the modules proved to be highly effective in protecting the solar cells against mechanical loads and distributing mechanical stress, as shown by minimal crack propagation and limited impact on overall module efficiency. Comparative analysis further indicates that Shingle-Matrix modules outperform conventional flat-ribbon and round-wire ribbon modules in combined SML and TC tests, while showing comparable degradation during DH testing. To further validate the implications given, a larger sample size should be utilized and i.e. the DH testing should be continued further to determine statistical robustness and performance over extended periods.

With continued development, shingle matrix technology has the potential to play a key role in the future of European solar module manufacturing, providing a highly reliable and visually appealing solution for sustainable energy generation in building integrated photovoltaic applications.

Data availability statement

The data supporting this study are not publicly available due to corporate confidentiality and intellectual property restrictions. For further inquiries, researchers may contact the corresponding author, but data access cannot be granted.

Competing interests

The author hereby declares no competing interests.

Acknowledgement

References

[1] N. Klasen, F. Lux, J. Weber, T. Roessler, and A. Kraft, "A Comprehensive Study of Module Layouts for Silicon Solar Cells Under Partial Shading," *IEEE J. Photovoltaics*, vol. 12, no. 2, pp. 546–556, Mar. 2022, doi: 10.1109/JPHOTOV.2022.3144635.

[2] *DIN EN IEC 61215:2021 - Terrestrial photovoltaic (PV) modules - Design qualification and type approval*, 2021.

[3] VDMA, "International Technology Roadmap for Photovoltaics (ITRPV) Re.2020." 2021.

[4] VDMA, "International Technology Roadmap for Photovoltaics (ITRPV) Re.2023." 2024.

[5] M. Schachinger, "Sinkende Topcon-Modulpreise machen PERC-Module bald unverkäuflich," PV-Magazine. Accessed: Aug. 15, 2024. [Online]. Available: https://www.pv-magazine.de/2024/05/21/sinkende-topcon-modulpreise-machen-perc-module-bald-unverkaeuflich/

[6] V. Nikitina *et al.*, "Shingling meets perovskite-silicon heterojunction tandem solar cells," *Solar Energy Materials and Solar Cells*, vol. 263, p. 112590, Dec. 2023, doi: 10.1016/j.solmat.2023.112590.

[7] *DIN EN IEC 61730:2016 Photovoltaic (PV) - Module Safety Qualification*, 2016.

[8] N. Klasen, F. Heinz, A. De Rose, T. Roessler, A. Kraft, and M. Kamlah, "Root cause analysis of solar cell cracks at shingle joints," *Solar Energy Materials and Solar Cells*, vol. 238, p. 111590, May 2022, doi: 10.1016/j.solmat.2022.111590.

[9] T. Rößler *et al.*, "Progress in shingle interconnection based on electrically conductive adhesives at Fraunhofer ISE," presented at the 2nd ESMAC-2021, 2022, p. 020012. doi: 10.1063/5.0127455.

[10] M. Foti *et al.*, "Silicon Heterojunction Solar Module using Shingle interconnection," in *2021 IEEE 48th Photovoltaic Specialists Conference (PVSC)*, Fort Lauderdale, FL, USA: IEEE, Jun. 2021, pp. 1092–1095. doi: 10.1109/PVSC43889.2021.9518670.

[11] P. Zahn, "Verbundvorhaben Shirkan – \." M10 Industries AG;, Freiburg, 2023. doi: 10.2314/KXP:1895997976.

[12] Solarwatt GmbH, "Datenblatt Panel Vision 60M construct." Jun. 01, 2024. [Online]. Available: https://www.solarwatt.de/canto/download/2cebbqabo90jj9vjke3c74jk1t

[13] Solarwatt GmbH, "Datenblatt Panel Vision GM 3.0 construct." Jul. 17, 2024. [Online]. Available: https://www.solarwatt.de/canto/download/o3o0pubrtt7cj326oq1nrgvt36

[14] N. A. Latif *et al.*, "Advancements in Shingle Matrix Technology for High Volume Production," in *2024 IEEE 52nd Photovoltaic Specialist Conference (PVSC)*, Seattle, WA, USA: IEEE, Jun. 2024, pp. 0605–0611. doi: 10.1109/PVSC57443.2024.10748959.

[15] J.-B. Charpentier, P. Voarino, and J. Gaume, "Ribbons lengthening induced by thermal cycling in PV modules, Part II: Glass-ribbon mechanical interaction through the encapsulant," *Solar Energy Materials and Solar Cells*, vol. 265, p. 112643, 2024, doi: 10.1016/j.solmat.2023.112643.

[16] A. J. Beinert, P. Romer, M. Heinrich, J. Aktaa, and H. Neuhaus, "Thermomechanical design rules for photovoltaic modules," *Progress in Photovoltaics: Research and Applications*, vol. 31, no. 12, pp. 1181–1193, 2023, doi: https://doi.org/10.1002/pip.3624.

[17] J. Irikawa, H. Hashimoto, H. Kanno, and M. Taguchi, "Correlation between damp-heat test and field operation for electrode corrosion in photovoltaic modules," *Solar Energy Materials and Solar Cells*, vol. 284, p. 113375, Jun. 2025, doi: 10.1016/j.solmat.2024.113375.